ADVANCED MATERIALS INTERFACES
www.advmatinterfaces.de

Ambient Plasma Synthesis of Si-Fe Hollow Nanoparticles and Their Biocompatibility and Lithium Storage Capacity

Jeong Hoon Byeon and Young-Woo Kim**

Si, the second most abundant element in the Earth's crust, is one of the most industrially important materials because of its unique semiconducting properties. Hence, it is highly sought and researched, driven by the demand for better materials for applications in electronics, sensors, catalysis, and in the biomedical sciences for diagnostics and therapeutics[1] since Si offers a good alternative to traditional materials since Si-based materials have been shown to exhibit minimal toxicity[2,3] and other superior physicochemical properties.[4,5]

Nanostructured Si materials such as nanoparticles, nanowires, nanotubes, and porous Si have shown unique chemical, optical, electronic, and mechanical properties distinct from those of the corresponding bulk materials, which give rise to their potential use in the fields of luminescence, catalysis, energy storage, and biomedical sciences.[6] Recently, hollow structured Si materials have been of further interest because of their low density, increased surface area and high porosity.[7]

Although it is challenging to blend multiple modalities into a single entity, multimodal nanoparticles offer hope in achieving this goal, and thus it is attractive to consider blending other materials into a single particle. As a robust, stable, environmentally green, and inexpensive material, an Si-Fe configuration could take a critical role in the next generation of nanomaterials with a wide range of potential applications.[8] For instance, formulations containing Si and Fe components would allow not only the contrast agents of magnetic resonance imaging (MRI), and the diagnosis and enucleation of tumors using MRI monitoring for the noninvasive and nondestructive imaging modality *in vivo,* but also the controlled transport and the egestion of nanoparticles circulating in the living body by applying an external magnetic field.[1] Furthermore, Si is an exciting and promising alternative anode material to replace carbon in Li-ion batteries due to its high gravimetric capacity of ≈4200 $mAhg^{-1}$, which is ten times higher than that of traditional graphite anode (≈370 $mAhg^{-1}$).[9] More recently, conducting Fe incorporated with Si nanoparticles to enhance the electron conductivity of Si nanoparticles and hence electrochemical performance has been previously reported.[10]

Dr. J. H. Byeon
Department of Chemistry
Purdue University
Indiana 47907, United States
E-mail: jbyeon@purdue.edu
Dr. Y.-W. Kim
Department of Automotive Engineering
Hoseo University
Asan 336-795, Republic of Korea
E-mail: ywkim@hoseo.edu

DOI: 10.1002/admi.201300134

Various synthetic strategies have been developed to prepare this type of nanostructured Si-based material such as template-directed synthesis, self-curing, solvent extraction, and so on. However, due to the high crystallization energy barrier of Si, these strategies can hardly be used to synthesize hollow structured Si; moreover, their processes are not environmentally benign and energy efficient.[6] Nonetheless, hollow structured Si has been made by chemical vapor deposition of Si precursors with hard templates,[11] and thermal decomposition of Si precursors.[12] These methods are usually high in cost and vacuum, and cannot be easily scaled up.

The present work introduces an ambient heterogeneous spark discharge to fabricate Si-Fe hollow nanoparticles for verifying their biocompatibility and lithium storage capacity regarding biomedical and energy storage purposes. The use of plasma discharges for nanoscale materials synthesis is a rapidly developing field. In particular, nonthermal plasmas at atmospheric pressure are attractive because of several factors conducive to efficiency.[13] Given that Si and Fe are nontoxic, it is also considered to be an environmentally friendly material compared to other low-cost inorganic materials.[14] Furthermore, the absence of liquid solvents together with the high thermal stability of gases involved in this process makes spark discharge an attractive alternative to produce Si-based nanomaterials.[15] The spark discharge is a kind of atmospheric-pressure nonequilibrium discharges. While the collision rate of electrons, ions, and neutrals is high, the discharge does not reach thermal equilibrium because it is short-lived, being interrupted before an arc discharge is formed through.[16] In a spark channel, high temperature vapor is generated from the melting tip of a Si rod. This vapor cools rapidly during diffusion to the region surrounding the spark. Primary particles are then formed by nucleation from the vapor. The primary particles generated by the nucleation grow through not only the condensation of Si atoms but also the coagulation caused by collisions between particles. A broad variety of Si-based building blocks with different shapes and compositions, similar to prospects accessible by liquid phase routes, is yet not accessible *via* an gas-phase route.[3] In our previous work, we reported the creation of different carbonaceous nanostructures by controlling the conditions of heterogeneous spark discharges.[17] The cooling rate in the spark is defined from a previous study,[17] and was –660 K s^{-1} in the present case. As a significant expansion of the previous study, this is the first attempt to synthesis Si-Fe hollow nanoparticles in a continuous gas-phase manner without using any wet chemical steps under ambient conditions.

A Si-Fe spark configuration in an N_2 gas flow environment was employed to produce Si-Fe hollow nanoparticles, and the nanoparticles were separated using mechanical filtration.

ADVANCED MATERIALS INTERFACES
www.advmatinterfaces.de

Materials Views
www.MaterialsViews.com

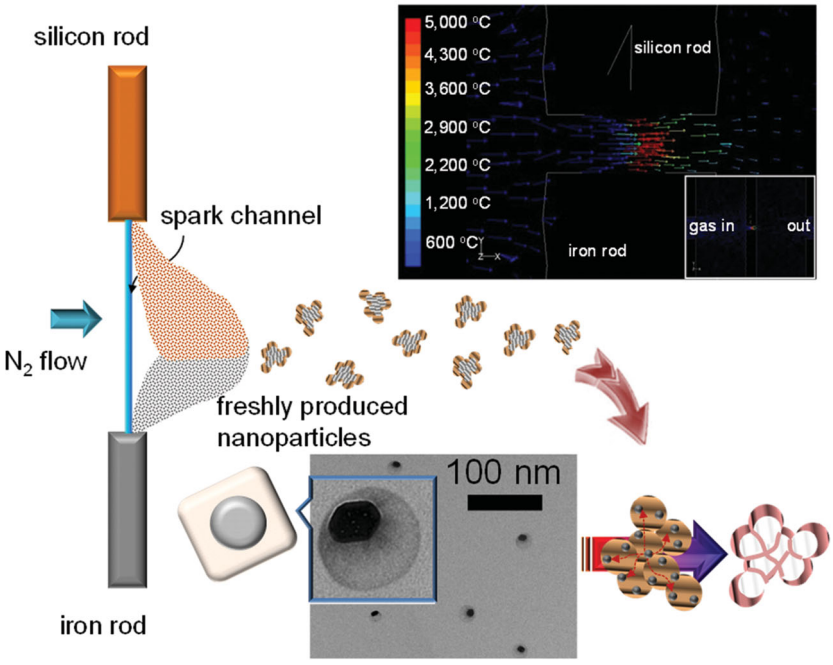

Scheme 1. Ambient heterogeneous spark discharge to synthesize Si-Fe hollow nanoparticles in the gas-phase. A temperature profile near the spark channel and TEM images of Si-Fe particles at a rapid condensation condition (cooling rate).

Finally, they were employed to measure their biocompatibility and lithium storage capacity. The as-synthesized hollow nanoparticles exhibited a biocompatibility (>83% cell viability) and a stable lithium storage performance (≈900 $mAhg^{-1}$) during the 200 charge-discharge cycles. The nontoxic Si incorporated structure showed good biocompatibility to human embryonic kidney (HEK) 293 cells, and furthermore, the ultrafine sizes (≈20 nm in lateral dimension) with hollow structure facilitated abundant space for efficient lithium storage and the buffering of large volume change during the repeated cycling.

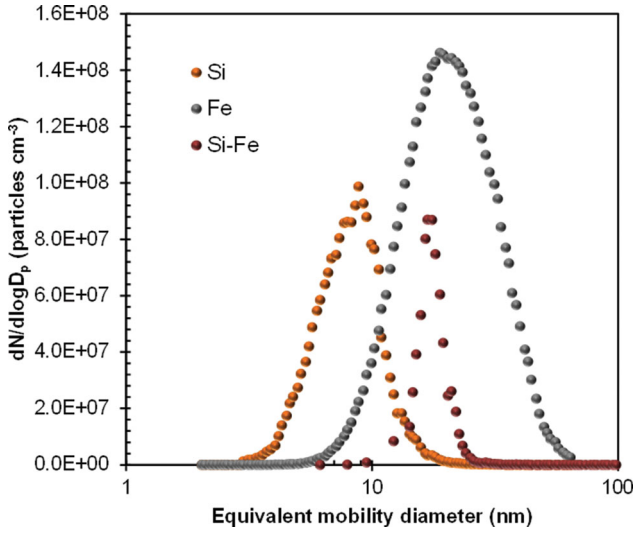

Figure 1. Size distributions of spark-produced individual Si and Fe particles, and their incorporated nanostructures (Si-Fe) in the gas-phase. Standard deviations are noted in Table 1.

The gas temperature inside the spark channel increased beyond a critical value of ≈3500 K, which was sufficient to sublimate parts of the Si and Fe electrodes.[18] The duration of each spark was very short and the vapors cooled rapidly downstream of the spark. This formed a supersaturation resulting in particle formation through nucleation-condensation. **Scheme 1** shows an example of rapid condensation (3300 K s^{-1} cooling rate, estimated from a numerical analysis as shown in Scheme 1) of Si-Fe hybrid particles from the spark channel; it can be seen in TEM images (also shown in Scheme 1) that a dark core and bright shell respectively corresponded to Fe and Si. The total number concentration (TNC), geometric mean diameter (GMD), and geometric standard deviation (GSD) of the Fe particles, which were measured using a scanning mobility particle sizer (SMPS, 3936, TSI, US), were 7.05×10^7 particles cm^{-3}, 20.3 nm, 1.52, respectively, as shown in **Figure 1**. Si-Fe nanoparticles were formed near the spark channel by incorporating Si with Fe under N_2 gas flow environment. We verified the incorporation of the Fe component within the Si matrix by measuring the size distributions of the Si and Si-Fe cases in the gas-phase. **Table 1** summarizes the size distribution measurements of the Si and Si-Fe cases. The TNC, GMD, and GSD of the Si-Fe case were 1.05×10^7 particles cm^{-3}, 18.3 nm and 1.24, respectively. The analogous data for Si were 2.94×10^7 cm^{-3}, 7.9 nm, and 1.36, respectively. The size distribution of the Si-Fe was shifted to larger sizes due to incorporation of Fe, and there was no bimodal distribution character, implying that the Si was nearly quantitatively incorporated with the Fe, to form the Si-Fe nanoparticles. Moreover, the size distribution shows a smaller degree of polydispersity revealing the homogeneous incorporation of Si and Fe components.

Low- and high-magnification transmission electron microscope (TEM, JEM-3010, JEOL, Japan) images show the morphology of Si, Fe, and Si-Fe samples (**Figure 2**). Specimens were prepared for examination in the TEM by direct electrostatic gas-phase sampling at a sampling flow of 1.0 L min^{-1} and an operating voltage of 5 kV using a Nano Particle Collector (NPC-10, HCT, Korea). The TEM images reveal that the Fe particles were agglomerates (≈26 nm in lateral dimension) of several primary particles, which is consistent with the SMPS

Table 1. A summary of the size distributions of spark-produced individual Si and Fe particles, and their incorporated nanostructures (Si-Fe) in the gas-phase.

Case	GMD (nm)	GSD (–)	TNC (particles cm^{-3})
Si	7.9	1.36	2.94×10^7
Fe	20.3	1.52	7.05×10^7
Si-Fe	18.3	1.24	1.05×10^7

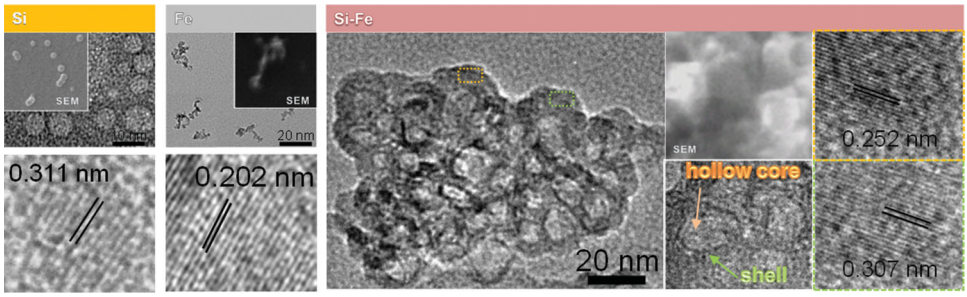

Figure 2. Low- and high-magnification TEM images of individual Si (8.8 ± 2.3) and Fe (26.1 ± 7.9) particles, and their incorporated nanostructures (Si-Fe, 21.8 ± 2.6). Representative SEM images of each sample are also displayed.

data (measured agglomerated Fe particles) noted in Table 1. As shown in the inset of Fe, about 0.202 nm size of the lattice fringe of Fe can be observed, which can be indexed as the (110) plane of the body-centered cubic structure. In the case of Si, visible lines confirm the presence of crystalline material; the spacing distance is 0.311 nm, close to the theoretical value of 0.313 nm between the (111) Si crystalline planes. It seems that the co-condensation of the vapors resulted in Fe incorporation with the Si matrix after the spark channel. The TEM image shows the larger sizes of the Si-Fe nanoparticles owing to gathering individual nanoparticles during the direct electrostatic gas-phase sampling. Nevertheless, the hollow structures were clearly seen and had about 0.307 and 0.252 nm in the *d*-spacing (see inset) on their shell region, which are corresponded to (220) and (422) lattice fringes of β-$FeSi_2$. While the scanning electron microscope (JSM-6500F, JEOL, Japan) image of the nanoparticles also shows bright spherical particles due to their hollow characteristics.

The formation mechanism of the Si-Fe hollow nanoparticles from the spark discharge is also summarized in Scheme 1. Due to the low melting temperature of Fe, it is reasonable to assume that Fe molten forms are formed first, and then the Si-Fe structures are formed later due to Fe diffusion into the Si matrix. The nucleated Si network suppresses the aggregation between the molten Fe particles, thus forming a uniform dispersion of Fe within the Si matrix. The low cooling rate led to high diffusion rates of molten Fe species in the gas-phase; hence, during Si precipitation, the molten Fe particles moved outward from the core due to a temperature gradient,[19] and thus, a cavity was formed inside the structures.

The X-ray diffractometry (RINT-2100, Rigaku, Japan) pattern peaks [from (220) to (042)] show crystalline planes of $FeSi_2$ (**Figure 3**), and the diffraction peaks at 2θ = 29.1° and 49.4° were attributed to orthorhombic β-$FeSi_2$ (220) and (422) (JCPDS 20–0532), respectively, which are consistent with the TEM observations. The Fe $2p_3$ peak of the X-ray photoelectron spectrum (Axis HIS, Kratos Analytical, Japan) appears at a binding energy of 708.2 eV which corresponds to β-$FeSi_2$. Other two features at lower binding energies at 99.7 and 99.0 eV can be assigned to Si $2p_{3/2}$ and $2p_{1/2}$ levels in β-$FeSi_2$.[20] Another inset of Figure 3 shows a magnetization curve with respect to the applied magnetic field at 300 K using 7404 Lake Shore Cryotronics device (US). The hollow nanoparticles did not show a hysteresis loop, implying that the particles are superparamagnetic. The absence of hysteresis is attributed to the small particle size and finite size effect in the nanoparticles.[8] The saturation magnetization of the nanoparticles was approximately 22 emu g^{-1}, and this magnetization value was less than that of the pure Fe nanoparticles (171 emu g^{-1}). This can be explained by considering the diamagnetic contribution of the Si components surrounding the Fe atoms. It is possible that surface magnetic anisotropy was changed with the existence of Si components, the surface spins disorientation increased, and thus the magnetic moment decreased.

To clarify whether the hollow nanoparticles exhibit good biocompatibility that can potentially be utilized for biomedical applications, the cytotoxicity of the hollow nanoparticles at different concentrations, such as 20, 50, 100, 200, 400 μg mL^{-1}, was evaluated by MTS assay in HEK 293 cells, in comparison with individual Si and Fe nanoparticles (**Figure 4**a). It was observed that the hollow nanoparticles exhibited a higher toxicity at a high particle concentration. The range of cell viability was about 83–96% for all the tested concentrations, which

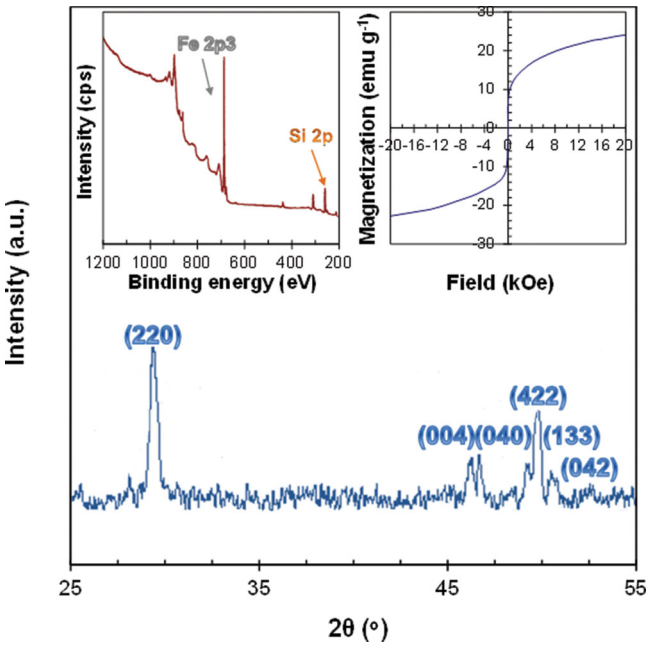

Figure 3. XRD, XPS (inset, left-side), and magnetization profiles (inset, right-side) of Si-Fe hollow nanoparticles. The nanoparticles were sampled on a hydrophobic polytetrafluoroethylene substrate through a mechanical filtration for the characterizations.

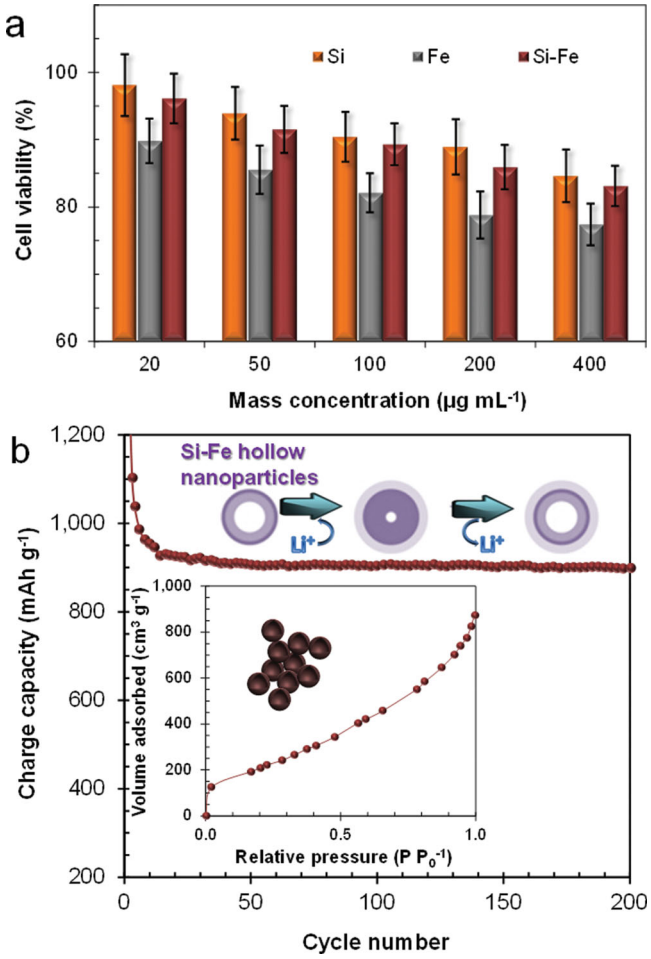

Figure 4. Cell cytotoxicity and lithium storage capacity of Si-Fe hollow nanoparticles. (a) In vitro cytotoxicity measurements of the Si-Fe nanoparticles including individual Si and Fe particles in HEK 293 cells. (b) Cyclic lithium storage performance for the Si-Fe hollow nanoparticles. Adsorption isotherms of the nanoparticles is also shown as the inset.

was similar to that observed for individual Si nanoparticles (84–98%). Nontoxic Si incorporation with Fe probably enhanced the biocompatibility of individual Fe nanoparticles, and the alloying, not simply Fe attaching on Si, might also be suitable to maintain low cytotoxicity by attenuating Fe diffusion into cell structures to be induced adverse effects due to high bond strength between Si and Fe.[21] This implies that the spark-produced hollow nanoparticles warrant further investigation.

As for an energy storage device, the cycle life is an important parameter to evaluate its performance. Therefore, we performed charge-discharge tests to examine the cycle life of the Si-Fe hollow nanoparticles electrode as a capacitor. Despite a drop in the initial stage, the charge capacity of the Si-Fe hollow nanoparticles still remained at ≈72% (≈900 $mAhg^{-1}$) of the initial value even after 200 cycles, highlighting an enhancement in cyclic performance, revealing the influence of a hollow structure with Fe atoms. Even though Si can and theoretically store energy at a capacity as high as 4200 $mAhg^{-1}$, the huge volume change (>300%) during the alloying-dealloying processes led to a drastic fading in capacity upon cycling. The elaborately fabricated Si-Fe structures might induce decrease of Si volume change during the processes, hence a high capacity remained after 200 cycles. N_2 adsorption measurements (via a Micromeritics ASAP 2010 apparatus) with the Brunauer, Emmett, and Teller method was used to determine the porosity of the hollow nanoparticles and to check the possibility of interconnected pores in the structures (inset of Figure 4b). The overall shapes of the samples indicate their meso- and macro-porous characteristics. The uptakes at >0.85 and <0.85 of P P_0^{-1} may originate from the void spaces among agglomerated hollow nanoparticles and the core areas of the nanoparticles, respectively.[22] The pores within the nanoparticles could show an appropriate structure as buffering spaces against the volume change of the particles upon the charge-discharge process and helping with ion transport, which eventually led to enhanced cyclic performances. Even though many factors may contribute to the decay, the main reason for the decrease of cyclic life may be due to a volume expansion produced by the charge-discharge (lithiation-delithiation, shown in the inset of Figure 4b) between the Li^+ and the nanoparticles (anode materials), leading to the pulverization and subsequent electrical disconnection of the electrodes.

We developed for the first time a continuous gas-phase synthesis of Si-Fe hollow nanoparticles through an ambient heterogeneous spark discharge without any wet chemical preparations, and we also tested their biocompatibility and lithium storage capacity. The Si incorporated structure could make their biocompatibility to mammalian cells, and furthermore, the ultrafine sizes with hollow structure facilitated abundant space for efficient lithium storage and the buffering of large volume change during repeated cycling. We believe this provides new perspectives and useful information for the design of efficient, low-cost, environmentally-friendly nanomaterials for biomedical (drug/gene carriers) and energy storage (anode materials in lithium ion batteries) applications.

Experimental Section

Spark Plasma: As shown in Scheme 1, a spark was generated between Si (diameter: 8 mm, length: 60 mm, Alfa Aesar, US) and Fe rods (diameter: 3 mm, length: 50 mm, Nilaco, Japan) inside a reactor within an N_2 flow environment at standard temperature and pressure. The specifications of the spark discharge were as follows: resistance, 0.5 MΩ; capacitance, 1.0 nF; loading current, 2.3 mA; applied voltage, 3.8 kV; and frequency, 1024 Hz. The flow rate of the gases was controlled by mass flow controllers (Kofloc, Japan), and the cooling rate was 660 K s^{-1}. The Si-Fe hollow nanoparticles were synthesized using the spark discharge, where the nanoparticles grow through co-condensation of Si vapor and Fe vapor. Once nuclei are generated, the vapors of the Si and Fe co-condense on the nuclei by heterogeneous condensation. The resulting nanoparitcles were separated from the flow via mechanical filtration. They were then set aside in a clean booth to keep them in powder form.

In Vitro Cytotoxicity: The cytotoxicity of the spark-produced nanoparticles was evaluated using HEK 293 cells by the MTS, 3-(4,5-dimethyl-thiazol-2-yl)-5-(3-carboxymethoxyphenyl)-2-(4-sulfophenyl)2H-tetrazolium, assay. This work employed HEK cells for cytotoxicity measurements, because these cells had already been employed to measure toxicity of inorganic nanoparticle based complexes.[23] The cells were cultured in 200 mL Dulbecco's modified eagle medium (Carlsbad, US) supplemented with 10% fetal bovine

serum at 37 °C, 5% CO_2, and 95% relative humidity. The cells were seeded in a 96-well microtiter plate (Nunc, Germany) at densities of 1×10^5 cells well^{-1}. After 24 h, the culture media were replaced with serum-supplemented culture media containing the nanoparticles (1 mg mL^{-1}), and the cells were incubated for 24 h. Then, 30 µL of the MTS reagent was added to each well. The cells were incubated for an additional 2 h. The absorbance was then measured using a microplate reader (Spectra Plus, TECAN, Switzerland) at a wavelength of 490 nm. The cell viability (%) was compared with that of the untreated control cells in media without nanoparticles and calculated with $[A]_{test}$:$[A]_{control} \times 100\%$, where $[A]_{test}$ is the absorbance of the wells with nanoparticles and $[A]_{control}$ is the absorbance of the control wells. All experiments were performed in triplicate, and the results were reported as average values and standard deviations.

Lithium Storage Capacity: The electrochemical measurements were carried out using a LAND CT2001 A battery tester with Li metal as the counter electrodes at room temperature. The fabricated Si-Fe hollow naonparticles were mixed with polyvinylidene fluoride, at a weight ratio of 90:10 in *N*-methyl-2-pyrrolidone to form a homogeneous slurry. The resultant slurry was then pasted on a copper foil substrate with a blade. The hollow nanoparticles loading density of the electrode was ca. 1.0 mg cm^{-2}. The prepared electrode sheets were placed in a vacuum at 80 °C to evaporate the solvent. CR2032-type coin cells were fabricated in a glove box with an argon atmosphere. The electrolyte was 1 M $LiPF_6$ in a 50:50 w/w mixture of ethylene carbonate and diethyl carbonate. The charge-discharge cycles of the cells were measured at a constant current density of 100 mAg^{-1} within a voltage range of 0–2.0 V.

Received: December 4, 2013
Revised: March 31, 2014
Published online: May 2, 2014

[1] M. P. Singh, T. M. Atkins, E. Muthuswamy, S. Kamali, C. Tu, A. Y. Louie, S. M. Kauzlarich, *ACS Nano* **2012**, *6*, 5596.
[2] K. Sato, S. Yokosuka, Y. Takigami, K. Hirakuri, K. Fujioka, Y. Manome, H. Sukegawa, H. Iwai, N. Fukata, *J. Am. Chem. Soc.* **2011**, *133*, 18626.
[3] R. Körmer, B. Butz, E. Spiecker, W. Peukert, *Cryst. Growth Des.* **2012**, *12*, 1330.
[4] Y. Yao, M. T. McDowell, I. Ryu, H. Wu, N. Liu, L. Hu, W. D. Nix, Y. Cui, *Nano Lett.* **2011**, *11*, 2949.
[5] J. W. Aptekar, M. C. Cassidy, A. C. Johnson, R. A. Barton, M. Lee, A. C. Ogier, C. Vo, M. N. Anahtar, Y. Ren, S. N. Bhatia, C. Ramanathan, D. G. Cory, A. L. Hill, R. W. Mair, M. S. Rosen, R. L. Walsworth, C. M. Marcus, *ACS Nano* **2009**, *3*, 4003.
[6] M.-P. Liu, C.-H. Li, H.-B. Du, X.-Z. You, *Chem. Commun.* **2012**, *48*, 4950.
[7] S. Tan, Q. Wu, J. Wang, Y. Wang, X. Liu, K. Sui, X. Deng, H. Wang, M. Wu, *Microporous Mesoporous Mat.* **2011**, *142*, 601.
[8] N. Dahal, V. Chikan, *Chem. Mater.* **2010**, *22*, 2892.
[9] H. Wu, G. Zheng, N. Liu, T. J. Carney, Y. Yang, Y. Cui, *Nano Lett.* **2012**, *12*, 904.
[10] H. Dong, R. X. Feng, X. P. Ai, Y. L. Cao, H. X. Yang, *Electrochim. Acta* **2004**, *49*, 5217.
[11] M.-H. Park, M. G. Kim, J. Joo, K. Kim, J. Kim, S. Ahn, Y. Cui, J. Cho, *Nano Lett.* **2009**, *9*, 3844.
[12] B. H. Ma, F. Cheng, J. Chen, J. Zhao, C. Li, Z. Tao, J. Liang, *Adv. Mater.* **2007**, *19*, 4067.
[13] D. Z. Pai, K. Ostrikov, S. Kumar, D. A. Lacoste, I. Levchenko, C. O. Laux, *Sci. Rep.* **2013**, *3*, 1221.
[14] A. S. W. Wong, D. Z. Chi, *J. Electrochem. Soc.* **2010**, *157*, H847.
[15] V. A. Vons, L. C. P. M. de Smet, D. Munao, A. Evirgen, E. M. Kelder, A. Schmidt-Ott, *J. Nanopart. Res.* **2011**, *13*, 4867.
[16] K. Ostrikov, E. C. Neyts, M. Meyyappan, *Adv. Phys.* **2013**, *62*, 113.
[17] J. H. Byeon, J.-W. Kim, *Appl. Phys. Lett.* **2010**, *96*, 153102.
[18] J. H. Byeon, J. H. Park, J. Hwang, *J. Aerosol Sci.* **2008**, *39*, 888.
[19] J. H. Byeon, J. H. Park, K. Y. Yoon, J. Hwang, *Nanoscale* **2009**, *1*, 339.
[20] F. Esaka, H. Yamamoto, N. Matsubayashi, Y. Yamada, M. Sasase, K. Yamaguchi, S. Shamoto, M. Magara, T. Kimura, *Appl. Surf. Sci.* **2010**, *256*, 3155.
[21] B. Egert, G. Panzner, *Phys. Rev. B* **1984**, *29*, 2091.
[22] R. Jia, J. Chen, J. Zhao, J. Zheng, C. Song, L. Li, Z. Zhu, *J. Mater. Chem.* **2010**, *20*, 10829.
[23] a) M. A. Vetten, N. Tlotleng, D. T. Rascher, A. Skepu, F. K. Keter, K. Boodhia, L.-A. Koekemoer, C. Andraos, R. Tshikhudo, M. Gulumian, *Part. Fib. Toxicol.* **2013**, *10*, 50; b) M. Sun, L. Yang, P. Jose, L. Wang, J. Zweit, *J. Mater. Chem. B* **2013**, *1*, 6137; c) P. Li, D. Li, L. Zhang, G. Li, E. Wang, *Biomaterials* **2008**, *29*, 3617.

